Materials Advances

ROYAL SOCIETY OF CHEMISTRY

PAPER

View Article Online
View Journal | View Issue

Cite this: *Mater. Adv.*, 2020, 1, 45

Potential for neutron and proton transmutation doping of GaN and Ga_2O_3†‡

Julie V. Logan, *[a] Elias B. Frantz,[b] Lilian K. Casias,[c] Michael P. Short,[a] Christian P. Morath[d] and Preston T. Webster[d]

Received 10th February 2020,
Accepted 11th February 2020

DOI: 10.1039/d0ma00017e

rsc.li/materials-advances

As the potential applications of GaN and Ga_2O_3 are limited by the inadequacy of conventional doping techniques, specifically when uniform selective area p-type doping is required, the potential for transmutation doping of these materials is analyzed. All transmuted element concentrations are reported as a function of time for several common proton and neutron radiation sources, showing that previously published results considered a small subset of the dopants produced. A 40 MeV proton accelerator is identified as the most effective transmutation doping source considered, with a 2.25×10^{17} protons per cm^2 fluence yielding net concentrations of uncompensated p-type dopants of 7.7×10^{15} and 8.1×10^{15} cm^{-3} for GaN and Ga_2O_3, respectively. Furthermore, it is shown that high energy proton accelerator spectra are capable of producing dopants required for magnetic and neutron detection applications, although not of the concentrations required for current applications using available irradiation methods.

1 Introduction

Wurtzite GaN and monoclinic β-Ga_2O_3 are direct wide and ultra-wide bandgap semiconductors with bandgaps of approximately 3.4 and 4.8 eV, respectively. While interest in these two semiconductor systems is growing, the development of some electronic devices using these materials is stalemated by the present inability to achieve selective area p-type doping. Conventional techniques; including selective area etch and regrowth, activation-enhanced laterally pattered ion implantation, and selective area diffusion; have been unable to produce junctions of the required quality for production of high performance vertical GaN transistors.[1] This work investigates the potential of transmutation doping as an alternative to circumvent this limitation impeding the use of GaN and Ga_2O_3 for some applications.

GaN has applications in optoelectronic, high-power, and high-frequency devices due to its large breakdown field, high electron mobility, and high converter power density in conjunction with its large heat capacity and thermal conductivity.[2] Particular applications include laser diodes, microwave RF power amplifiers, high voltage switching devices, UV photodetectors, Schottky rectifiers, and solar cells.[2,3] Interest in Ga_2O_3 stems from its predicted critical field of 6–8 MV cm^{-1},[4] which is more than double that of GaN and SiC, allowing for high current and voltage (up to 10 kV) power transistor operation. Furthermore, low cost, high quality, scalable melt-grown substrates make Ga_2O_3 one of the few ultra-wide bandgap materials that is predicted to compete with wide bandgap materials like GaN and SiC for power and RF device applications.[4,5]

Both GaN and Ga_2O_3 are also being investigated for use as dilute magnetic semiconductors (DMS) due to these materials' capacity to achieve room temperature ferromagnetism when doped with transition and rare-earth metals. If adequately doped to a few atomic percent, these materials have applications such as spin-based transistors, spin valves, magnetic memories, and spin-polarized light-emitting diodes.[6] Examples of applicable transition metal dopants potentially produced from transmutation include Co, Ni, and Cu.[7,8] Additionally, proper doping permits use of these materials in more cost-effective and robust thermal neutron detectors. Doping of either of these radiation-tolerant material systems with 6-Li or 10-B permits fabrication of neutron scintillators and semiconductor thermal neutron detectors.[2]

All electronic device architectures and applications mentioned above require selective semiconductor doping to permit control of carrier concentrations, but in contrast to Si and GaAs, there are not yet well-established, technologically advanced doping methods for wide-bandgap semiconductors.[1,4,9] The high bond strength and rigid lattice structure of wide bandgap materials make it difficult to achieve incorporation of substitutional impurities. This makes common doping methods which seek to insert atoms into the lattice through diffusion, implantation, or otherwise, practically

[a] *Department of Nuclear Science and Engineering, Massachusetts Institute of Technology, Cambridge, USA. E-mail: jvl2xv@mit.edu*
[b] *Department of Engineering Science & Mechanics, The Pennsylvania State University, State College, USA*
[c] *Quantum Phenomena Division, Sandia National Laboratories, Albuquerque, USA*
[d] *Space Vehicles Directorate, Air Force Research Laboratory, Kirtland Air Force Base, USA*

† All data, scripts, and intermediate analysis files can be found on our GitHub repository for this manuscript https://github.com/jvl2xv/GaN_Ga2O3_TransmutationDoping. See DOI: 10.5281/zenodo.3462165

‡ Electronic supplementary information (ESI) available. See DOI: 10.1039/d0ma00017e

demanding. Specifically for GaN, the primary acceptor dopant is Mg and effective p-type doping is difficult because Mg incorporation is complicated, Mg has a large ionization energy of 170–220 eV, and Mg is readily passivated by hydrogen incorporation and nitrogen vacancies.[10–13] For Ga_2O_3, there are no known shallow acceptors and the general consensus in the community is that conventional doping means will not be effective in producing p-type samples.[4] Furthermore, producing uniform heavily doped wafers of these materials is limited by the involved nature of the conventional doping methods. However, one feasible method for doping, which is well-suited to permit uniform and selective area doping, has not yet been conclusively explored for these wide bandgap semiconductors: transmutation doping.[1]

As protons and neutrons move through a semiconductor, they lose energy primarily through elastic or inelastic scattering events with the host nuclei in the case of neutrons and with host nuclei and electrons in the case of protons. Alternatively, these baryons may interact with lattice atoms through nuclear reactions, resulting in the production of excited lattice atom nuclei of a different composition. The decay of these nuclei to lower energy states over time may be associated with the emission of particles (proton(s), neutron(s), electron(s), positron(s)) or high energy gamma rays. This process can result in the production of an atom of a different element within the lattice, doping the semiconductor. The efficiencies of different nuclear reactions and the probabilities of different decays are influenced by the original lattice atom nucleus as well as the energy and identity of the incident particle initiating the reaction.[14] Transmutation doping is fundamentally different from implantation doping in that implantation doping relies on injecting a foreign nucleus into the lattice while transmutation doping is the transformation of one native lattice atom into another, the dopant. Transmutation doping is particularly effective for doping as effective dopants typically lie adjacent to the host lattice atom on the periodic table and these are the nuclei which are more likely formed through the decay of excited lattice nuclei.

Neutron and proton transmutation doping are methods capable of producing a high-quality doped semiconductor in terms of doping precision and homogeneity.[15,16] Neutron transmutation doped Si has the best quality among all doping methods.[17] Dopant concentration precision is achieved because the impurity concentration produced is linearly proportional to the neutron or proton fluence. Precision doping with errors of $<1\%$ are readily achievable for neutron transmutation of Si, a well-established process.[16,17] Doping precision is important for applications in which highly resistive materials are required, such as avalanche detectors as well as more generally when highly controlled junctions are required as in CMOS fabrication.[16,18,19] Both neutron and proton transmutation doping produce more uniform dopant profiles than does ion implantation doping because neutrons and protons both produce dopants along their entire track, in comparison to ion implantation in which dopants are only produced at the end of the incident particle track. Neutron transmutation doping is the most uniform doping mechanism available due to the small probability of a transmutation reaction, the highly penetrating nature of neutrons, the uniformity of neutron flux achievable, and the random isotopic distribution of host nuclei in the sample. Doping uniformity across an entire ingot is achievable.[17] Neutron transmutation doped semiconductors do not exhibit the microresistivity structure commonly exhibited by conventionally doped materials. Furthermore, for applications requiring large-scale uniformity, neutron transmutation does not exhibit the doping gradients across the wafer produced by traditional doping methods. For example, float zone doped Si yields slices with four to ten times higher radial resistivity gradient than does neutron transmutation doping.[16] This uniformity of doping is important for a variety of devices, but finds its most prominent advantage in high power devices such as thyristors (such as integrated gate-commutated thyristors and gate turn-off thyristors) and insulated-gate bipolar transistors due to the functionality requirements of low on-resistance and high breakdown voltage.[17,20] Additionally, the defects generated through neutron transmutation doping can generally be annealed and the dopants activated through relatively low temperature annealing (particularly when compared to ion implantation doping).[16,21]

Neutron transmutation doping is a method which produces uniform concentrations of impurity atoms in semiconductors and is employed commercially for high power silicon device production.[22] There have been no published theoretical or experimental investigations of the potential of transmutation doping of Ga_2O_3 and, although there have been a few experimental investigations of the potential for the use of thermal neutron transmutation to dope GaN, no effort has conducted a complete analysis considering all impurities introduced due to the irradiation and their temporal variation. In the earliest experimental investigations in 2002 and 2004,[23,24] Ge production through (n,γ) reactions with the two stable isotopes of gallium was considered in the interpretation of experimental results. Later, the (n,p) reaction of neutrons with 14-N was included in the analysis after observing that high sample resistivity (10^8 Ohms at room temperature) was maintained after 1000 °C annealing.[25] There exists no analysis including other thermal neutron reactions, fast neutron reactions, or the temporal variation in impurities produced.[26,27] Additionally, the use of protons for transmutation doping has not been considered for these wide-bandgap materials. This work addresses all of these shortcomings.

A comprehensive analysis of the fundamental potential for transmutation doping of GaN and Ga_2O_3, wide bandgap semiconductors, is conducted. All nuclear reactions that produce impurities, their temporal variation, and the potential of non-thermal neutron and proton-induced transmutation are considered. All transmuted elemental concentrations are presented as a function of time following irradiation using a variety of proton and neutron sources, enabling analysis of the use of these techniques for doping to control carrier transport, magnetic properties, and neutron detection capabilities of these materials.

2 Methods

The following neutron and proton transmutation irradiation scenarios are considered: monoenergetic proton irradiation,

Table 1 Summary of neutron spectra considered in the transmutation analysis in terms of the number of bins that the original spectrum was composed of and a short description of the source

Spectrum name	Bins	Spectrum description
EBR-2	29	Experimental breeder reactor spectrum
252-Cf	70	252-Cf spontaneous fission source
BWR-MOX-Gd-40GWd	1102	BWR MOX fuel with Gd, 40 GWd per THM
PWR-MOX-40GWd	1102	PWR MOX fuel with Gd, 40 GWd per THM
PWR-UO2-40GWd	1102	PWR UO_2 fuel, 40 GWd per THM
Phenix	172	Fast breeder reactor, Phénix
ITER-DD	175	Magnetic confinement fusion, ITER D-D
ITER-DT	175	Magnetic confinement fusion, ITER D-T
JAEA-FNS	175	JAEA fusion neutron source D-T
HFIR-highres	238	Mat. test reactor, ORNL HFIR midplane
All-fast	3	1 MeV neutrons source
All-thermal	3	0.025 eV neutron source

typical of an accelerator source, of 2, 5, 10, 20, 30, and 40 MeV and neutron irradiation from a variety of potential neutron sources, which are summarized in Table 1. These neutron spectra are visualized in Fig. 1. For all proton spectra, a total fluence of 2.25×10^{17} protons per cm^2 is employed (associated with 1 hour irradiation with a 10 μA accelerator with a 1 cm^2 spot size). For all neutron spectra, 3.6×10^{17} neutrons per cm^2 are considered, a fluence associated with 1 hour irradiation in a typical light water reactor of total 10^{14} neutrons per cm^2 per s scalar flux.

The FISPACT-II enhanced multiphysics inventory and nuclear observables system, a code validated and maintained by the UK Atomic Energy Authority, is utilized to quantify the total elemental transmutation.[51] This code computes charged-particle and neutron transmutation and activation using published natural abundances, cross-sections, and decay data, and has previously been validated for semiconductor transmutation applications by comparison to experiments and GEANT4 simulations.[52] FISPACT employs the most up-to-date published nuclear data from the TENDL-2017, HEIR-0.1, ENDF/B.VIII.0, JEFF-3.3, JENDL-4.0, and CENDL-3.1 international libraries.[51] Specifically for this application, the FISPACT 2017 TENDL database is used for proton (gxs-162) and neutron (gxs-709) nuclear reaction cross-sections, the UKAEDD-12 decay library is used for decay data, and the UKFY-4.1 library (as obtained from JEFF-3.1.1 decay data) is used for fission yields. The use of these nuclear reaction cross-sectional databases implies that input proton and neutron spectra are binned into 162 and 709 equal lethargy bins, respectively.[51] It should be noted that, as the published proton cross-section databases do not contain uncertainty quantification for proton reactions, no uncertainties can be derived from this deterministic code. The validity of the results is determined by the accuracy of the cross-section libraries employed.

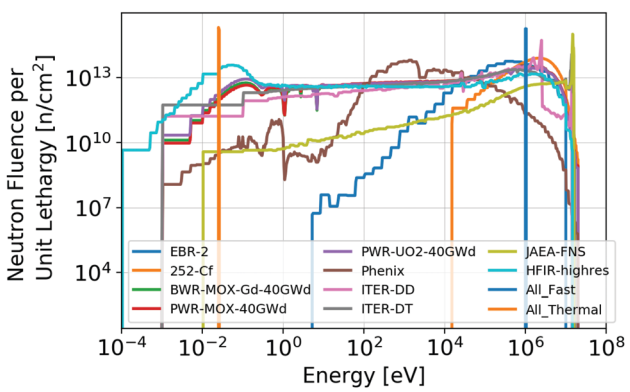

Fig. 1 Incident neutron spectra, each of which is used as a source for transmutation quantification. More detail concerning these spectra is included in Table 1. For all neutron spectra shown here, the total fluence of 3.6×10^{17} neutrons per cm^2 is employed (1 hour irradiation in a typical light water reactor of total 10^{14} neutrons per cm^2 per s scalar flux).

The nuclear libraries are condensed by FISPACT-II, given the incident radiation spectrum being analyzed. A deterministic, stiff set of coupled ordinary differential rate equations are then solved, the solutions of which provide the time-dependent transmutation of the initial set of nuclides in the sample caused by the input radiation and by spontaneous radioactive decay. The equation governing the concentration, $N_i(t)$ of nuclide i is given in eqn (1) where the summation is conducted over all nuclides.

$$\frac{dN_i(t)}{dt} = \sum_j \left\{ \left(\lambda_i^j + \sigma_i^j \phi^{\text{int}}(t) \right) N_j \right\}, \quad (1)$$

In eqn (1), σ_i^j [cm^2] is the condensed cross-section for production of isotope i from isotope j (a negative value representing destruction equal to the total cross-section for isotope j if $i = j$), ϕ^{int} [cm^{-2} s^{-1}] is the energy-integrated projectile flux (required due to the use of condensed cross-sections), and λ_i^j [s^{-1}] is the decay constant of isotope j to isotope i (a negative value representing destruction equal to the total decay constant for isotope j if $i = j$).[51]

3 Results and discussion

3.1 Validation with experiment

To experimentally validate transmuted concentration results in these semiconductors, comparison is made to previous experiment where an unintentionally doped GaN sample was irradiated with thermal and fast neutron fluences each of 1.5×10^{17} neutrons per cm^2 from a thermal neutron pool-type light water moderated and cooled WWR-c reactor, yielding a dopant concentration of 2.2×10^{16} Ge atoms per cm^3.[26] As the precise WWR-c neutron

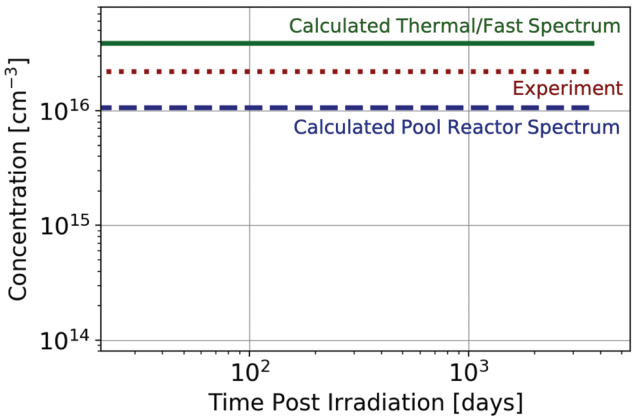

Fig. 2 Comparison between experimentally observed[26] and computed Ge concentration resulting from GaN neutron irradiation with thermal and fast neutron fluence of 1.5×10^{17} neutrons per cm^2 for pure thermal and pure fast neutron spectra and for a similar thermal pool-type light water reactor as was used for experimental irradiation. Concentrations are shown starting at 3 weeks post-irradiation, as this was when the experiment was performed.

spectrum used in the experiment was unavailable, a pure thermal spectrum (0.025 eV) and pure fast spectrum (1 MeV) of the stated fluences and a spectrum from another thermal pool-type light water reactor (LWR) of equivalent total fluence are assumed. Given that both are thermal LWRs and the moderation mechanism is the same for this reactor and that utilized in experiment, one would anticipate that the neutron spectra are similar. The comparison of the computed Ge concentration (from each neutron spectrum) with the experimental 2.2×10^{16} Ge atoms per cm^3 is shown in Fig. 2. As the experimental characterization occurred greater than 3 weeks following irradiation, the concentration is plotted starting at 3 weeks post-irradiation. It is observed that the experimental concentrations fall within the concentrations predicted by this work, which have approximately stabilized during this time interval.

3.2 Temporal transmuted element concentrations

The concentrations of impurities produced as a function of time under proton and neutron irradiation respectively are visualized for GaN in Fig. 3 and 4 and for Ga_2O_3 in Fig. 5 and 6. It is observed that many additional impurities are produced in concentrations comparable to the historically considered Ge and C.[23–27] Additionally, some elemental concentrations show substantial temporal dependence on the order of days to months. This defines the timescale for future experimental study of the doping of these systems through transmutation. It should be noted that these impurities are generally not located on the same site as the parent atom from which they originate due to the subsequent gamma and beta radioactive decays that occur, the energy of which is shared between the emitted particle and the nucleus, causing it to recoil.[23] The semiconductor activity (rate of these nuclear decays) as a function of time following irradiation is presented in the ESI.‡

3.3 Suitability of transmutation doping for applications

The suitability of neutron and proton irradiation for causing the transmutation required for p-type doping, magnetic applications, and neutron detection applications will now be reviewed.

In order to realistically impact semiconductor carrier populations, the compensation of dopants must be considered. As such, the difference between the p-type dopant concentration and the n-type dopant concentration introduced by transmutation is calculated. Many studies used to attribute p-type or n-type character to an impurity consist of density functional theory (DFT) simulations and, while more accurate hybrid functional simulations were chosen when available, there are potential sources of error arising from these simulation sources. Furthermore, the following assumptions are made: all dopants reside on their parent sublattice site (no interstitial or antisite defects) and the crystal is fully annealed (no radiation-induced compensating self-interstitials or vacancies). Deep levels are included in n- or

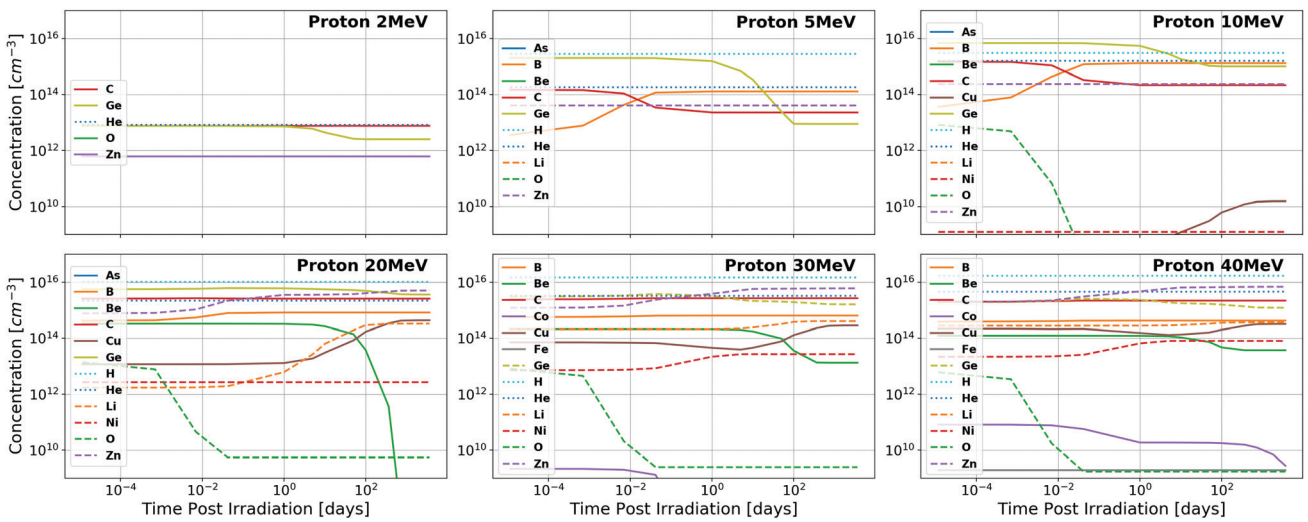

Fig. 3 Total concentrations of impurity elements introduced in GaN as a function of time following quasi-monoenergetic 2, 5, 10, 20, 30, and 40 MeV proton irradiation. Substantial dopants of note include Ge, B, C, and Zn for most proton energies (E_p), with the inclusion of Cu, Li, and Ni for $E_p \geq 20$ MeV and Be for $E_p \geq 30$ MeV. All results are shown in tabular format in the ESI.‡

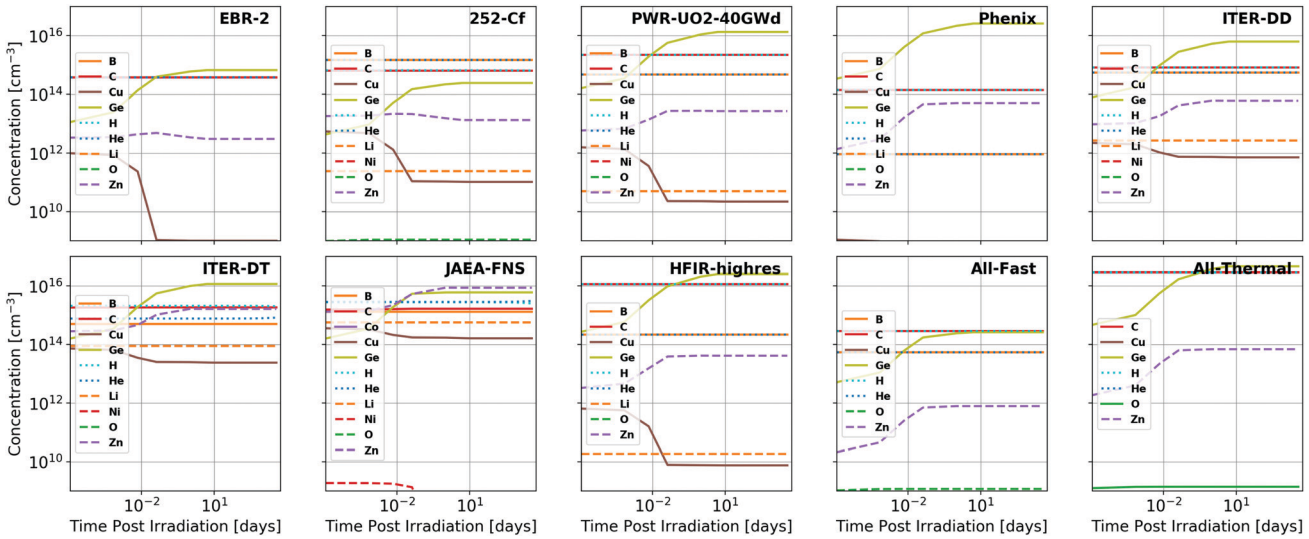

Fig. 4 Total concentrations of impurity elements introduced in GaN as a function of time following neutron irradiation, the spectra of which are summarized in Fig. 1. Substantial dopants of note include Ge, B, C, and Zn for most neutron spectra, with the inclusion of Cu and Li in the JAEA-FNS and ITER-DT spectra. The fission power reactor spectra (PWR-UO2-40GWd, BWR-MOX-Gd-40GWd, and PWR-MOX-40GWd) all produce nearly indistinguishable impurity concentration trends and, thus, only the PWR-UO2-40GWd results are visualized. All results are shown in tabular format in the ESI.‡

p-type attribution because their effective depth is Fermi level dependent, their depth may be overestimated in the DFT results, and because they are still employed to control semiconductor electrical conductivity (for example Fe in Ga_2O_3 producing a semi-insulating material[4]). Despite the potential sources of error in this attribution, Fig. 3–6 can be used to generate net doping introduced as a function of time for one's specific application. This attribution may be irradiation scenario dependent, as different amounts of damage and annealing can impact the site upon which the transmuted elements reside, which impacts their energy level and their resulting doping character. The dominant source of error in this attribution is likely the assumed position of the impurities within the lattice. With all of these potential sources of error in mind, the attributions used in this analysis of GaN and Ga_2O_3 doping are contained in Tables 2 and 3 respectively.

Impurities produced in transmutation are binned using Tables 2 and 3 to produce the total n- and p-type concentration of impurities introduced as a function of time, as shown for proton and neutron irradiation spectra respectively in Tables 4 and 5 for GaN and in Tables 6 and 7 for Ga_2O_3 at 50 days post one hour irradiation. It is observed that the samples become bulk n-type or are approximately compensated for the majority of irradiation scenarios. The full temporal variability is presented in the ESI.‡ Exceptions in which net dominant p-type doping is

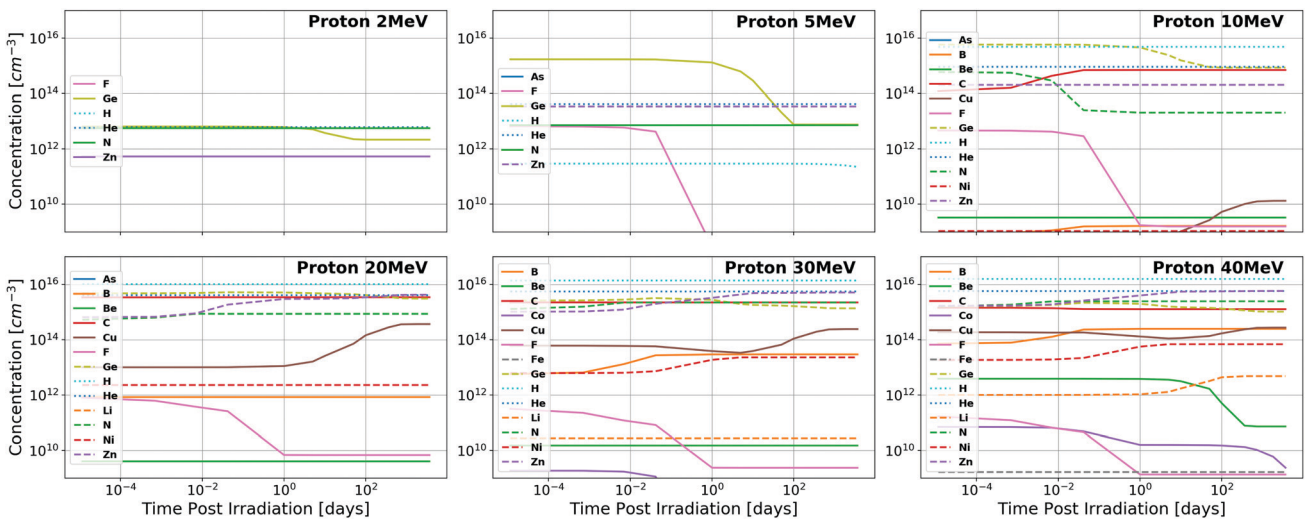

Fig. 5 Total concentrations of impurity elements introduced in Ga_2O_3 as a function of time following quasi-monoenergetic 2, 5, 10, 20, 30, and 40 MeV proton irradiation. Substantial dopants of note include Ge, N, and Zn for most proton energies (E_p), with the inclusion of C for $E_p \geq 10$ MeV, Cu and Ni for $E_p \geq 20$ MeV, B for $E_p \geq 30$ MeV, and Li for $E_p \geq 40$ MeV. All results are shown in tabular format in the ESI.‡

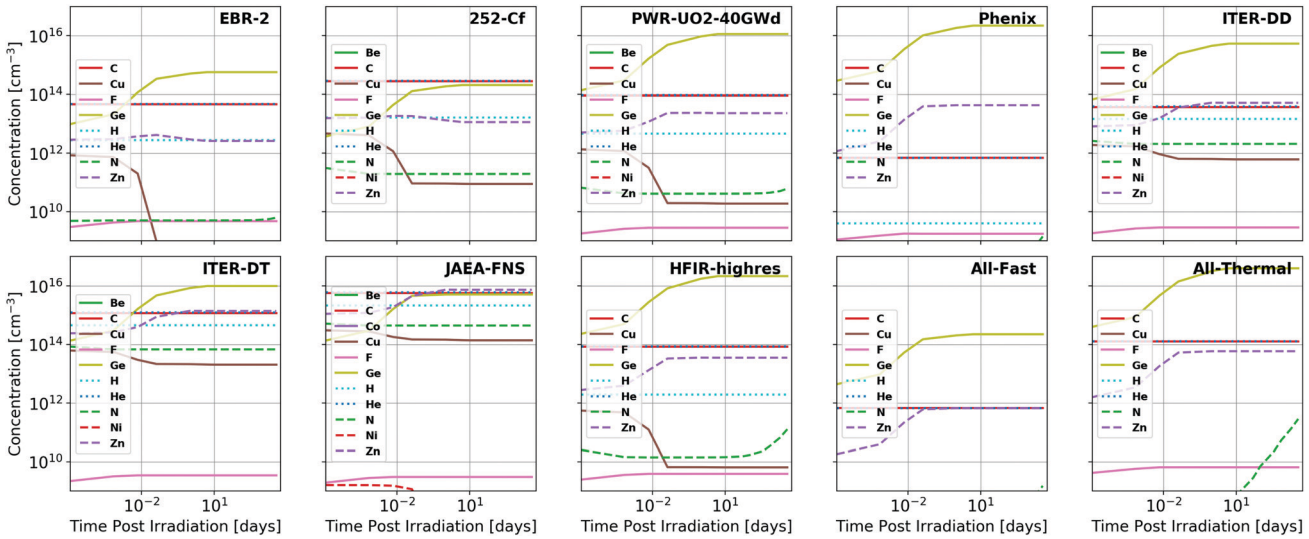

Fig. 6 Total concentrations of impurity elements introduced in Ga_2O_3 as a function of time following neutron irradiation, the spectra of which are summarized in Fig. 1. Substantial dopants of note include Ge, C, and Zn for most neutron spectra with additional production of Cu and N in JAEA-FNS, ITER-DD, and ITER-DT spectra. The fission power reactor spectra (PWR-UO2-40GWd, BWR-MOX-Gd-40GWd, and PWR-MOX-40GWd) all produce nearly indistinguishable impurity concentration trends and, thus, only the PWR-UO2-40GWd results are visualized. All results are shown in tabular format in the ESI.‡

Table 2 Doping character attribution of transmuted elemental impurities produced in GaN. For donors, energies are given with reference to the conduction band and for acceptors, energies are given with reference to the valence band

	Type	Attribution notes
H	—	Complex form determines nature[28]
He	—	
Li	p	Deep acceptor 2.23 eV[29]
Be	p	Predicted 0.060 eV,[30,31] but deep acceptor 2.16 eV Observed,[29,32] reduces p-type Mg depth to 0.170 eV[33]
B	—	No sources available
C	p	Deep acceptor 0.9 eV (DFT), 1 eV (experiment)[34–36]
O	n	Shallow donor on N, acceptor on interstitial or O_{Ga} site[37]
Fe	p	Deep acceptor 3.17 eV[38–41]
Co	—	No sources available
Ni	p	Activates Mg (p-type) dopants (H desorption)[42]
Cu	p	Deep acceptor 2.4 eV, p-type observed[43–45]
Zn	p	Deep acceptor 0.364 eV (DFT), 0.34 eV (experiment)[46]
Ge	n	Shallow donor 0.03 eV[28]
As	n	Deep donor 2.6–2.7 eV[47–50]

Table 3 Doping character attribution of transmuted elemental impurities produced in Ga_2O_3. For donors, energies are given with reference to the conduction band and for acceptors, energies are given with reference to the valence band

	Type	Attribution notes
H	—	Complex form determines nature[28]
He	—	No sources available
Li	p	Deep acceptor 1.6–1.9 eV[53]
Be	p	Deep acceptor[54]
B	—	No sources available
C	p	Deep acceptor >2 eV[4,55,56]
N	p	Deep acceptor 1.33 eV[57]
F	n	Shallow donor[58]
Fe	p	Deep acceptor 3.9–4.0 eV[59,60]
Co	—	Deep acceptor >2 eV[4,55,56]
Ni	p	Deep acceptor 0.76 eV[54]
Cu	p	Deep acceptor 0.96 eV[54,61,62]
Zn	p	Deep acceptor 0.33 eV (DFT), <0.5 eV (experiment)[54,63,64]
Ge	n	Shallow donor 0.01–0.03 eV[60,65]
As	—	No sources available

observed exist for GaN and Ga_2O_3 when irradiated with JAEA-FNS neutrons (a D-T fusion neutron source), 252-Cf neutrons (spontaneous fission) or protons of 2, 5, 20, 30, and 40 MeV. This trend of increasing p-type doping with increasing proton energy occurs because the probabilities of proton interactions generally peak at $10x$ MeV where x is the number of neutrons emitted from the unstable nucleus through the (p, xn) reaction.[52] Because of this, higher energy protons will be more likely to form a nucleus with a proton to neutron ratio that is too high to be stable. This will result in subsequent β^+ decay, which converts protons to neutrons and produces lower atomic number elements. These elements will likely contribute to p-type doping by acting as acceptors relative to the parent nucleus.

It should be noted that the neutron fluence employed in this computation (3.6×10^{17} neutrons per cm^2) was chosen with reactor fluxes in mind, which is unrealistic for current accelerator-based D-T generators, which would require over 100 hours of continuous operation to achieve this fluence.[66,67] For a 252-Cf source of 10 grams, 55 hours of continuous irradiation at a distance of 1 cm would be required.[68] The dopant population becomes more p-type as a function of time as the dominant n-type dopant Ge decays. Originally, the Ge isotopes 68-Ge, 69-Ge, and 70-Ge are produced in approximately equal amounts and 69-Ge decays to stable 69-Ga through β^+ decay with a half-life of 1.63 days, thus reducing the n-type dopant concentration. Additionally, the p-type dopant concentration is increased due to production of 67-Zn through the electron capture decay of 67-Ga with a half-life of 3.26 days. This temporal variability of electrical properties illustrates the importance of a holistic analysis when considering transmutation doping.

Table 4 Concentrations of introduced gross n-type, p-type, and net (compensated) p-type transmuted elemental impurities in existence at 50 days following quasi-monoenergetic 2, 5, 10, 20, 30, and 40 MeV proton irradiation of GaN. Attributions are made according to Table 2. The full temporal variation of n-type and p-type concentrations can be found in the ESI

	Induced dopant concentration in GaN [cm^{-3}]		
Source	p-Type	n-Type	Net p-type
P-2MeV	8.4×10^{12}	2.6×10^{12}	5.7×10^{12}
P-5MeV	6.4×10^{13}	2.5×10^{13}	3.9×10^{13}
P-10MeV	4.6×10^{14}	1.1×10^{15}	-6.0×10^{14}
P-20MeV	6.7×10^{15}	5.2×10^{15}	1.5×10^{15}
P-30MeV	9.0×10^{15}	2.0×10^{15}	7.0×10^{15}
P-40MeV	9.4×10^{15}	1.7×10^{15}	7.7×10^{15}

Table 5 Concentrations of introduced gross n-type, p-type, and net (compensated) p-type transmuted elemental impurities in existence at 50 days following neutron irradiation of GaN, the spectra of which are summarized in Fig. 1. Attributions are made according to Table 2. The full temporal variation of n-type and p-type concentrations can be found in the ESI

	Induced dopant concentration in GaN [cm^{-3}]		
Source	p-Type	n-Type	Net p-type
EBR-2	3.8×10^{14}	6.7×10^{14}	-2.9×10^{14}
252-Cf	6.5×10^{14}	2.4×10^{14}	4.1×10^{14}
BWR-MOX-Gd-40GWd	1.6×10^{15}	1.3×10^{16}	-1.1×10^{16}
PWR-MOX-40GWd	1.4×10^{15}	1.3×10^{16}	-1.1×10^{16}
PWR-UO2-40GWd	2.3×10^{15}	1.4×10^{16}	-1.1×10^{16}
Phenix	1.9×10^{14}	2.6×10^{16}	-2.6×10^{16}
ITER-DD	8.9×10^{14}	6.3×10^{15}	-5.4×10^{15}
ITER-DT	3.6×10^{15}	1.2×10^{16}	-8.1×10^{15}
JAEA-FNS	1.1×10^{16}	6.1×10^{15}	5.1×10^{15}
HFIR-highres	1.2×10^{16}	2.6×10^{16}	-1.4×10^{16}
All-fast	2.9×10^{14}	2.6×10^{14}	2.6×10^{13}
All-thermal	2.9×10^{16}	4.6×10^{16}	-1.7×10^{16}

Table 6 Concentrations of introduced gross n-type, p-type, and net (compensated) p-type transmuted elemental impurities in existence at 50 days following quasi-monoenergetic 2, 5, 10, 20, 30, and 40 MeV proton irradiation of Ga_2O_3. Attributions are made according to Table 3. The full temporal variation of n-type and p-type concentrations can be found in the ESI

	Induced dopant concentration in Ga_2O_3 [cm^{-3}]		
Source	p-Type	n-Type	Net p-type
P-2MeV	6.2×10^{12}	2.3×10^{12}	3.9×10^{12}
P-5MeV	4.2×10^{13}	2.1×10^{13}	2.1×10^{13}
P-10MeV	9.3×10^{14}	9.0×10^{14}	3.4×10^{13}
P-20MeV	7.6×10^{15}	4.5×10^{15}	3.1×10^{15}
P-30MeV	9.5×10^{15}	1.7×10^{15}	7.8×10^{15}
P-40MeV	9.6×10^{15}	1.4×10^{15}	8.1×10^{15}

Table 7 Concentrations of introduced gross n-type, p-type, and net (compensated) p-type transmuted elemental impurities in existence at 50 days following neutron irradiation of Ga_2O_3, the spectra of which are summarized in Fig. 1. Attributions are made according to Table 3. The full temporal variation of n-type and p-type concentrations can be found in the ESI

	Induced dopant concentration in Ga_2O_3 [cm^{-3}]		
Source	p-Type	n-Type	Net p-type
EBR-2	4.9×10^{13}	5.7×10^{14}	-5.2×10^{14}
252-Cf	2.9×10^{14}	2.1×10^{14}	8.4×10^{13}
BWR-MOX-Gd-40GWd	1.2×10^{14}	1.1×10^{16}	-1.1×10^{16}
PWR-MOX-40GWd	1.2×10^{14}	1.1×10^{16}	-1.1×10^{16}
PWR-UO2-40GWd	1.2×10^{14}	1.2×10^{16}	-1.1×10^{16}
Phenix	4.4×10^{13}	2.2×10^{16}	-2.2×10^{16}
ITER-DD	9.3×10^{13}	5.4×10^{15}	-5.3×10^{15}
ITER-DT	2.7×10^{15}	1.0×10^{16}	-7.4×10^{15}
JAEA-FNS	1.4×10^{16}	5.2×10^{15}	8.6×10^{15}
HFIR-highres	1.2×10^{14}	2.2×10^{16}	-2.2×10^{16}
All-fast	1.3×10^{12}	2.3×10^{14}	-2.2×10^{14}
All-thermal	1.9×10^{14}	3.9×10^{16}	-3.9×10^{16}

As mentioned in Section 1, transition metal doping of GaN and Ga_2O_3 can lead to room temperature ferromagnetism. Specifically in Fig. 3 and 4 it is observed that long-lived Fe, Co, Ni, and Cu are produced in GaN due to transmutation. For proton irradiation of 20 MeV and above, concentrations of $>10^{12}$ cm^{-3} and $>10^{13}$ cm^{-3} of Ni and Cu respectively are produced per hour. Neutrons are less effective at causing transition metal doping with the primary irradiations of note being the two D-T fusion sources producing Cu concentrations of $>10^{12}$ cm^{-3}. Similar results are observed in Fig. 5 and 6 for Ga_2O_3, due to the fact that the transmuted metallic constituents derive from the Ga present in both semiconductors. Given current applications, this doping efficiency is insufficient to provide the few atomic percent mole fractions required to produce DMS.[6–8]

Many neutron detection applications rely primarily on the large cross-section of interaction for neutrons with 10-B and 6-Li.[69] It is observed that protons are efficient at producing these two isotopes in GaN and Ga_2O_3. As both of these isotopes are radioactively stable, their concentration is invariant with time after they are produced. It is found that in GaN, protons with energies >30 MeV are capable of producing concentrations of $>10^{14}$ cm^{-3} of 6-Li and 10-B per hour of irradiation. In Ga_2O_3, concentrations only exceed 10^{12} cm^{-3} for B-10 from 40 MeV protons. This difference arises because 10-B and 6-Li are transmuted from the anion, which is not common between the two semiconductors. The uniform production of neutron-sensitive isotopes through transmutation is desirable because the neutron reaction products must travel to and deposit energy in the active region of the detector, a requirement which sets an intrinsic limit to the efficiency of a 6-Li or 10-B coated semiconductor detectors to 4.5%.[70] Despite this, the concentrations produced through transmutation are unsuitable for thermal neutron detection applications as they result in intrinsic detection efficiencies, given an assumed 1 cm thick absorber layer, of <0.001%.

4 Conclusion

The potential for transmutation doping of GaN and Ga_2O_3 is presented, as unresolved doping difficulties restrict the use of these materials, specifically when p-type doping is required. All transmuted element concentrations are reported as a function of time, showing the substantial temporal variability of the semiconductor composition. A range of realistically obtainable

proton and neutron spectra are considered, as originating from accelerators, fission reactors, fusion reactors and reactions, and radioactive isotopes. It is shown that, for the impurity attribution considered in this analysis, most proton spectra as well as 252-Cf spontaneous fission and D-T fusion neutron spectra are capable of producing a net increase in p-type dopants which increases with time as Ge decays and Zn is produced. At 50 days following a one hour irradiation, the net concentration of uncompensated p-type dopants introduced is 7.7×10^{15} and 8.1×10^{15} cm^{-3} for GaN and Ga_2O_3 respectively for the most effective irradiation considered (40 MeV protons). Furthermore, it is shown that high energy proton accelerator spectra are capable of producing Cu, a key dopant for magnetic applications, in concentrations of $>10^{13}$ cm^{-3} per hour in both semiconductors, but this efficiency is orders of magnitude too small to effectively produce dilute magnetic semiconductors. Finally, concentrations of $>10^{14}$ cm^{-3} of key neutron detection isotopes are produced in GaN per hour through similar high energy proton irradiation, but these concentrations are again too small for current neutron detector implementations.

Conflicts of interest

There are no conflicts to declare.

Acknowledgements

The present work has benefited from the financial support of the US Department of Defense SMART Fellowship.

Notes and references

1 I. C. Kizilyalli, E. P. Carlson, D. W. Cunningham, J. S. Manser, Y. Xu and A. Y. Liu, *Wide Band-Gap Semiconductor Based Power Electronics for Energy Efficiency*, 2018, pp. 1–17.
2 C. Zhou, A. Ghods, V. G. Saravade, P. V. Patel, K. L. Yunghans, C. Ferguson, Y. Feng, B. Kucukgok, N. Lu and I. T. Ferguson, *ECS J. Solid State Sci. Technol.*, 2017, **6**, Q149–Q156.
3 K. N. Chopra, *Lat. Am. J. Phys. Educ.*, 2014, **8**, 541–547.
4 M. Tadjer, J. L. Lyons, N. Nepal, J. A. Freitas, A. D. Koehler and G. M. Foster, *ECS J. Solid State Sci. Technol.*, 2019, **8**, Q3187–Q3194.
5 Z. Galazka, *Semicond. Sci. Technol.*, 2018, **33**, 113001.
6 S. A. Chambers and B. Gallagher, *New J. Phys.*, 2008, **10**, 055004.
7 P. R. Ganz, C. Sürgers, G. Fischer and D. M. Schaadt, *J. Phys.: Conf. Ser.*, 2010, **200**, 062006.
8 M. Shakil, A. Husain, M. Zafar, S. Ahmad, M. Khan, M. Masood and A. Majid, *Chin. J. Phys.*, 2018, **56**, 1570–1577.
9 M. G. Pravica, N. A. Guardala and J. L. Price, *Diamond Relat. Mater.*, 2009, **18**, 846–849.
10 J. K. Sheu and G. C. Chi, *J. Phys.: Condens. Matter*, 2002, **14**, R657–R702.
11 Y.-T. Shi, F.-F. Ren, W.-Z. Xu, X. Chen, J. Ye, L. Li, D. Zhou, R. Zhang, Y. Zheng, H. H. Tan, C. Jagadish and H. Lu, *Sci. Rep.*, 2019, **9**, 8796.
12 M. Tadjer, B. Feigelson, J. Greenlee, J. A. Freitas, T. J. Anderson, J. Hite, L. Ruppalt, C. R. Eddy, K. Hobart and F. J. Kub, *ECS J. Solid State Sci. Technol.*, 2016, **5**, P124–P127.
13 J. Chen, W. Yi, T. Kimura, S. Takashima, M. Edo and T. Sekiguchi, *Appl. Phys. Express*, 2019, **12**, 051010.
14 K. Krane, *Introductory Nuclear Physics*, Wiley, 1987.
15 S. Kang and H. Cho, Method for doping gallium Nitride (GaN) substrates and the resulting doped gan substrate, 2002.
16 J. M. Meese, in *The NTD Process – A New Reactor Technology*, ed. J. M. Meese, Springer US, Boston, MA, 1979, pp. 1–10.
17 M. Kim, S. Park and I. Lim, *2009 13th European Conference on Power Electronics and Applications*, 2009, pp. 1–10.
18 S. H. Park, T. W. Kang and T. W. Kim, *J. Mater. Sci.*, 2004, **39**, 3217–3219.
19 J. Montserrat, J. Bausells, E. Lora-Tamayo and F. Serra-Mestres, *Vacuum*, 1989, **39**, 687–690.
20 J. W. Cleland, K. Lark-Horovitz and J. C. Pigg, *Phys. Rev.*, 1950, **78**, 814–815.
21 S. H. Park, T. W. Kang and T. W. Kim, *J. Mater. Sci.*, 2004, **39**, 6353–6355.
22 S. B. Duun, A. B. Nielsen, C. Hendrichsen, T. Sveigaard, O. T. Andersen, J. J. Jabłoński and L. A. Jensen, Neutron Transmutation Doped (NTD) Silicon for High Power Electronics, Topsil Semiconductor Materials, 2013.
23 K. Kuriyama, T. Tokumasu, J. Takahashi, H. Kondo and M. Okada, *Appl. Phys. Lett.*, 2002, **80**, 3328–3330.
24 K. Kuriyama, T. Tokumasu, H. Sano and M. Okada, *Solid State Commun.*, 2004, **131**, 31–35.
25 T. Nakamura, K. Kamioka, K. Kuriyama, K. Kushida, Q. Xu and M. Hasegawa, *Solid State Commun.*, 2015, **205**, 1–3.
26 A. Y. Polyakov, N. B. Smirnov, A. V. Govorkov, N. G. Kolin, D. I. Merkurisov, V. M. Boiko, A. V. Korulin and S. J. Pearton, *J. Vac. Sci. Technol., B: Nanotechnol. Microelectron.: Mater., Process., Meas., Phenom.*, 2010, **28**, 608–612.
27 S. Park, T. Kang and T. W. Kim, *J. Mater. Sci.*, 2004, **39**, 6353–6355.
28 M. Reshchikov and H. Morkoç, *J. Appl. Phys.*, 2005, **97**, 061301.
29 J. Pankove, M. Duffy, E. Miller and J. Berkeyheiser, *J. Lumin.*, 1973, **8**, 89–93.
30 F. Bernardini, V. Fiorentini and A. Bosin, *Appl. Phys. Lett.*, 1997, **70**, 2990–2992.
31 Y. Nakano and T. Jimbo, *Appl. Phys. Lett.*, 2002, **81**, 3990–3992.
32 F. Albrecht, U. Reislöhner, G. Pasold, C. Hülsen, W. Witthuhn, J. Grillenberger and M. Dietrich, *Appl. Phys. Lett.*, 2004, **84**, 3876–3878.
33 C.-C. Yu, C.-F. Chu, J.-Y. Tsai, C.-F. Lin, W.-H. Lan, C.-I. Chiang and S.-C. Wang, *Jpn. J. Appl. Phys.*, 2001, **40**, L417–L419.
34 J. Hu, Y. Zhang, M. Sun, D. Piedra, N. Chowdhury and T. Palacios, *Mater. Sci. Semicond. Process.*, 2018, **78**, 75–84.
35 L. Li, J. Yu, Z. Hao, L. Wang, J. Wang, Y. Han, H. Li, B. Xiong, C. Sun and Y. Luo, *Comput. Mater. Sci.*, 2017, **129**, 49–54.
36 J. L. Lyons, A. Janotti and C. G. Van de Walle, *Phys. Rev. B: Condens. Matter Mater. Phys.*, 2014, **89**, 035204.

37 A. F. Wright, *J. Appl. Phys.*, 2005, **98**, 103531.
38 S. Heikman, S. Keller, T. Mates, S. DenBaars and U. Mishra, *J. Cryst. Grow.*, 2003, **248**, 513–517.
39 R. Heitz, P. Maxim, L. Eckey, P. Thurian, A. Hoffmann, I. Broser, K. Pressel and B. K. Meyer, *Phys. Rev. B: Condens. Matter Mater. Phys.*, 1997, **55**, 4382–4387.
40 M. Iwinska, R. Piotrzkowski, E. Litwin-Staszewska, T. Sochacki, M. Amilusik, M. Fijalkowski, B. Lucznik and M. Bockowski, *Appl. Phys. Express*, 2016, **10**, 011003.
41 J. L. Lyons, A. Janotti and C. G. Van de Walle, *Phys. Rev. B: Condens. Matter Mater. Phys.*, 2014, **89**, 035204.
42 I. Waki, H. Fujioka, M. Oshima, H. Miki and M. Okuyama, *J. Cryst. Grow.*, 2002, **234**, 459–462.
43 J. Senawiratne, M. Strassburg, A. Payne, A. Asghar, W. Fenwick, N. Li, I. Ferguson and N. Dietz, *MRS Online Proc. Libr.*, 2005, **892**, 0892-FF23-08.
44 K. Yohannes and D.-H. Kuo, *Mater. Sci. Semicond. Process.*, 2015, **29**, 288–293.
45 S. W. Kim, Y. H. Park, I. Kim, T.-E. Park, B. W. Kwon, W. K. Choi and H.-J. Choi, *Nanoscale*, 2013, **5**, 8550–8554.
46 S. Fischer, C. Wetzel, E. E. Haller and B. K. Meyer, *Appl. Phys. Lett.*, 1995, **67**, 1298–1300.
47 C. G. Van de Walle and J. Neugebauer, *Appl. Phys. Lett.*, 2000, **76**, 1009–1011.
48 J. I. Pankove and J. A. Hutchby, *J. Appl. Phys.*, 1976, **47**, 5387–5390.
49 L. J. Guido, P. Mitev, M. Gherasimova and B. Gaffey, *Appl. Phys. Lett.*, 1998, **72**, 2005–2007.
50 X. Li, S. Kim, E. E. Reuter, S. G. Bishop and J. J. Coleman, *Appl. Phys. Lett.*, 1998, **72**, 1990–1992.
51 J.-C. Sublet, *The FISPACT-II User Manual*, 2015.
52 J. V. Logan, M. P. Short, P. T. Webster, C. P. Morath and E. H. Steenbergen, *J. Mater. Chem. C*, 2019, **7**, 8905–8914.
53 A. Kyrtsos, M. Matsubara and E. Bellotti, *Appl. Phys. Lett.*, 2018, **112**, 032108.
54 C. Tang, J. Sun, N. Lin, Z. Jia, W. Mu, X. Tao and X. Zhao, *RSC Adv.*, 2016, **6**, 78322–78334.
55 J. L. Lyons, D. Steiauf, A. Janotti and C. G. Van de Walle, *Phys. Rev. Appl.*, 2014, **2**, 064005.
56 S. Lany, *APL Mater.*, 2018, **6**, 046103.
57 L. Dong, R. Jia, C. Li, B. Xin and Y. Zhang, *J. Alloys Compd.*, 2017, **712**, 379–385.
58 J. Yan and C. Qu, *J. Semicond.*, 2016, **37**, 042002.
59 M. E. Ingebrigtsen, J. B. Varley, A. Y. Kuznetsov, B. G. Svensson, G. Alfieri, A. Mihaila, U. Badstübner and L. Vines, *Appl. Phys. Lett.*, 2018, **112**, 042104.
60 A. T. Neal, S. Mou, S. Rafique, H. Zhao, E. Ahmadi, J. S. Speck, K. T. Stevens, J. D. Blevins, D. B. Thomson, N. Moser, K. D. Chabak and G. H. Jessen, *Appl. Phys. Lett.*, 2018, **113**, 062101.
61 C. Zhang, F. Liao, X. Liang, H. Gong, Q. Liu, L. Li, X. Qin, X. Huang and C. Huang, *Phys. B*, 2019, **562**, 124–130.
62 Y. Zhang, J. Yan, Q. Li, C. Qu, L. Zhang and W. Xie, *Mater. Sci. Eng., B*, 2011, **176**, 846–849.
63 X. Wang, F. Zhang, K. Saito, T. Tanaka, M. Nishio and Q. Guo, *J. Phys. Chem. Solids*, 2014, **75**, 1201–1204.
64 X. Wang, F. Zhang, K. Saito, T. Tanaka, M. Nishio and Q. Guo, *J. Phys. Chem. Solids*, 2014, **75**, 1201–1204.
65 J. B. Varley, J. R. Weber, A. Janotti and C. G. Van de Walle, *Appl. Phys. Lett.*, 2010, **97**, 142106.
66 C. Konno, K. Ochiai, M. Wada and S. Sato, *Fusion Eng. Des.*, 2008, **83**, 1774–1781.
67 A. Klix, T. DÖring, A. R. Domula and K. Zuber, *EPJ Web Conf.*, 2018, **170**, 02004.
68 R. Radev and T. McLean, *Neutron Sources for Standard-Based Testing*, Department of Energy Technical Report, 2014.
69 G. Knoll, *Radiation Detection and Measurement*, Wiley, 2000, pp. 505–522.
70 D. McGregor, M. Hammig, Y.-H. Yang, H. Gersch and R. Klann, *Nucl. Instrum. Methods Phys. Res., Sect. A*, 2003, **500**, 272–308.